Quantification of the Raf-C1 Interaction With Solid-Supported Bilayers

Andreas Eing,[b] Andreas Janshoff,[c] Hans-Joachim Galla,[b] Christoph Block,[d] and Claudia Steinem*[a]

*By use of the quartz crystal microbalance technique, the interaction of the Raf–Ras binding domain (RafRBD) and the cysteine-rich domain Raf-C1 with lipids was quantified by using solid-supported bilayers immobilized on gold electrodes deposited on 5 MHz quartz plates. Solid-supported lipid bilayers were composed of an initial octanethiol monolayer chemisorbed on gold and a physisorbed phospholipid monolayer varying in its lipid composition as the outermost layer. The integrity of bilayer preparation was monitored by impedance spectroscopy. For binding experiments, a protein construct comprising the RafRBD and Raf-C1 linked to the maltose binding protein and a His tag, termed MBP-Raf-C1, was used. Dissociation constants and rate constants of the association and dissociation were obtained for various 1,2-dimyristoyl-*sn*-glycero-3-phosphocholine (DMPC)/1,2-dimyristoyl-*sn*-glycero-3-phosphoserine (DMPS) lipid mixtures. Independently of the phosphatidylserine (PS) content, the dissociation constants were in the order of 5×10^{-7} M, while the on-rate constants were in the range of 2×10^{3} $(M s)^{-1}$ and the off-rate constants in the range of 1×10^{-3} s^{-1}. The maximum frequency shift increased significantly with increasing amounts of DMPS; this indicates that this negatively charged lipid is the primary binding site for MBP-Raf-C1. Exchange of DMPS for 1,2-dimyristoyl-*sn*-glycero-3-phosphoglycerol (DMPG) did not alter the thermodynamics and kinetics of protein binding, which implies that the protein interaction is mainly electrostatically driven. Scanning force microscopy (SFM) was employed to render protein adsorption visible and to confirm the assumption of a protein monolayer on the lipid layer. SFM images clearly revealed that the protein binds preferentially, but not solely, to negatively charged phosphatidylserine headgroups. We hypothesize that PS-enriched domains are initial binding sites with high affinity for Raf-C1, but that lateral interactions may account for protein domain growth.*

KEYWORDS:

biosensors · quartz crystal microbalance · Raf kinase · scanning probe microscopy · solid-supported bilayers

Introduction

The Ras/Raf/MEK/ERK cascade plays a pivotal role in the regulation of cell growth and differentiation. One major constituent of this cascade is Raf, a member of the serine/threonine protein kinase family that mediates signals from the cell surface to the nucleus by activation of the mitogen-activated protein kinase.[1–3] A critical step in the activation of Raf is its interaction with membrane-anchored Ras, a small GTPase, through its Raf–Ras binding domain (RafRBD). In vivo, in its active GTP-bound state, Ras recruits Raf to the plasma membrane, which is the first step in Raf activation.[4–6] However, Ras interaction alone is not sufficient to activate Raf kinase; other events such as Raf phosphorylation may also be required.[3]

Although little is known about the mechanism of Raf activation, the structure of Raf is well resolved. Three isoforms of Raf can be distinguished in mammals: A-Raf, B-Raf, and C-Raf-1, the last being the best studied.[7] C-Raf-1 consists of an N-terminal noncatalytic region and a C-terminal kinase domain (Figure 1 A). If the N-terminal region is missing (v-Raf oncoprotein), the kinase is constitutively active; this indicates that the N-terminal part locks the kinase in an inactive conformation and so is responsible for its regulation.[8] The noncatalytic N-terminus of Raf is composed of two regions (CR1 and CR2) that are highly conserved between different members of the Raf family. The first conserved region (CR1) consists of two modules, the RafRBD (amino acids 51–131) and a C1-type, cysteine-rich domain (Raf-C1, amino acids 139–184). While Ras binding to the RafRBD is well understood, the role of the Raf-C1 domain has remained elusive. Raf-C1 is a structural homologue of the protein kinase C phorbol ester binding domain that exhibits the zinc-finger motif. Four cysteine residues within the amino acid sequence

[a] *Prof. Dr. C. Steinem*
Institut für Analytische Chemie, Chemo- und Biosensorik
Universität Regensburg
93040 Regensburg (Germany)
Fax: (+49) 941-943-4491
E-mail: claudia.steinem@chemie.uni-regensburg.de

[b] *Dr. A. Eing, Prof. Dr. H.-J. Galla*
Institut für Biochemie
Westfälische Wilhelms-Universität
Wilhelm-Klemm-Strasse 2, 48149 Münster (Germany)

[c] *Prof. Dr. A. Janshoff*
Institut für Physikalische Chemie
Johannes-Gutenberg-Universität
Welderweg 11, 55128 Mainz (Germany)

[d] *Dr. C. Block*
Max-Planck Institut für Molekulare Physiologie
Otto-Hahn-Strasse 11, 44227 Dortmund (Germany)

  1439-4227/02/03/02-03 $ 17.50+.50/0 ChemBioChem **2002**, 3, 190–197

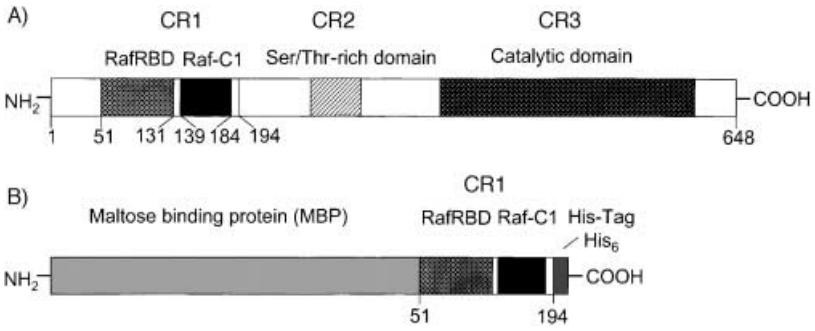

Figure 1. *A) Schematic drawing of the structure of full-length c-Raf-1. The protein is composed of three conserved regions: CR1, CR2, and CR3. CR1 comprises the Raf – Ras binding domain (RafRBD) and the cysteine-rich domain termed Raf-C1. CR2 is a serine/threonine-rich domain, which is a phosphorylation site. CR3 is the catalytic domain located near the C terminus. B) Schematic representation of the protein construct used in this study. CR1, incorporating amino acids 51—193, which comprise RafRBD and RafC1, is fused to a maltose binding protein. A His tag composed of six histidine residues is added at the C terminus to facilitate purification of the protein construct.*

$CX_2CX_9CX_2C$, together with two histidine residues, complex two zinc ions with high affinity.[9–13] Structurally, Raf-C1 resembles a protein kinase C of the aPKC category. In contrast to both cPKCs and nPKCs, aPKCs contain only one cysteine-rich domain and their activity is not affected by diacylglycerol or phorbol esters. It was demonstrated that Raf-C1 also interacts with neither diacylglycerol nor phorbol esters.[14, 15] However, it cannot be ruled out that an unidentified lipid cofactor, such as a ceramide, might interact with Raf-C1 instead.[16, 17] Evidence for such a cofactor is the fact that Raf cannot be fully activated by Ras in vitro. Despite these similarities between PKCs and Raf-C1, only a few studies have addressed the role of Raf-C1 in lipid binding. A possible interaction between Raf-C1 and phospholipids was investigated by vesicle binding experiments and microtiter plate assays. Ghosh et al.[14] showed that Raf-C1 interacts with vesicles containing phosphatidylserine and Improta-Brears et al.[18] found supporting results when they used an enzyme-linked immunosorbant assay (ELISA) based on lipid-covered microtiter plates. However, quantification of protein binding with these assays is rather difficult and binding kinetics cannot be obtained.

Lipid bilayers immobilized in a highly ordered fashion on a solid support in conjunction with appropriate transducers have, however, been proven to be well suited for study of lipid – protein interactions in a quantitative fashion.[19] Different preparation techniques to prepare these so-called solid-supported membranes are available.[19] The Langmuir – Blodgett and Langmuir–Schäfer techniques and techniques based on the chemisorption of thiol or disulfide components, for instance, are appropriate for immobilization of lipid bilayers on gold surfaces. Common techniques with which to study lipid – protein interactions on solid supports are optical (ellipsometry, surface plasmon resonance spectroscopy, interferometry) and electrochemical methods (cyclovoltammetry, impedance spectroscopy). Besides these well-established techniques, the quartz crystal microbalance (QCM) has also been recognized in recent years as a new versatile and label-free technique with which to follow adsorption processes at solid/liquid interfaces in chemical and biological research. For a current review on the quartz crystal microbalance and its applications in biosensing, see Janshoff et al.[20]

The objective of this study was to develop a quantitative in vitro assay—based on solid-supported bilayers in conjunction with the quartz crystal microbalance technique—for the determination of thermodynamic and kinetic data for interactions between Raf-C1 and lipid bilayers. The influence of variations in the lipid bilayer composition on the binding behavior of Raf-C1 was investigated. To corroborate the obtained results, in situ scanning force microscopy was utilized to visualize binding of Raf-C1 to solid-supported membranes.

Results

Binding of Raf-C1 to DMPC/DMPS

Since isolation of functional full-length c-Raf-1 had not as yet been successful and we were mainly interested in the interaction between Raf-C1 and lipid membranes, we used a protein construct composed of amino acids 51 – 194, incorporating the RafRBD and Raf-C1 components, fused to a maltose binding protein (MBP) at the N terminus to improve its solubility and a His Tag containing six histidine residues at the C terminus (Figure 1 B). This protein construct is termed MBP-Raf-C1. The molecular structure of amino acids 51 – 194 has been determined by NMR spectroscopy[15, 21] and ensures proper folding of the domains.

Lipid bilayers composed of a first chemisorbed octanethiol monolayer and a second phospholipid monolayer subsequently fused onto the first one were prepared on the gold surface of a quartz plate for binding experiments (Figure 2). Characteristic

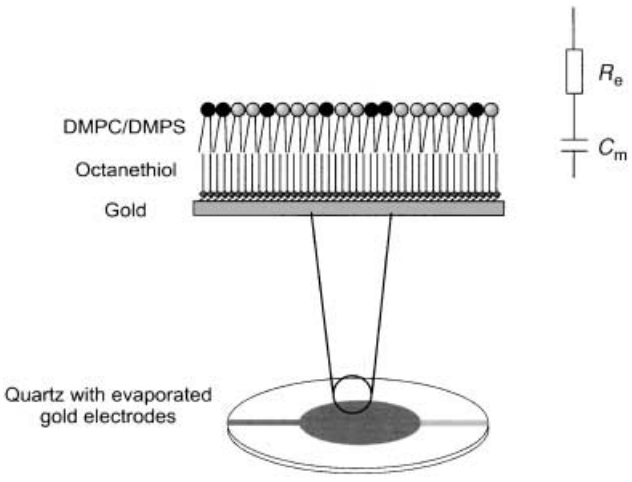

Figure 2. *Schematic representation of a functionalized quartz surface with an immobilized lipid bilayer composed of an octanethiol monolayer and a physisorbed phospholipid monolayer. The equivalent circuit on the right-hand side was used for impedance data evaluation. C_m represents the capacitance of the alkanethiol monolayer and the bilayer composed of the alkanethiol and a phospholipid, respectively, and R_e represents the Ohmic resistance of the electrolyte and the wire connections.*

electrical parameters of the octanethiol monolayer and the lipid bilayer can routinely be determined from the impedance spectra by means of impedance analysis, to ensure reproducible bilayer preparations. For data evaluation, an equivalent circuit composed of a capacitance C_m representing the octanethiol monolayer was used in series with an Ohmic resistance R_e to represent the bulk resistance and the wire connections (Figure 2). This equivalent circuit is valid, as octanethiol forms almost defect-free monolayers, resulting in a solely capacitive behavior in the observed frequency range.[22] By fitting the equivalent circuit to the data, the capacitance of the octanethiol monolayer was determined to be $(2.1 \pm 0.2)\ \mu F\,cm^{-2}$. After formation of the hydrophobic monolayer, vesicles composed of 1,2-dimyristoyl-*sn*-glycero-3-phosphocholine (DMPC) and 1,2-dimyristoyl-*sn*-glycero-3-phosphoserine (DMPS) were fused to form the second layer and impedance spectra were taken again. Data evaluation was conducted by using the same equivalent circuit. In this case, C_m represents the capacitance of the lipid bilayer. The assumption of a series connection of the capacitances of the two monolayers allows the specific capacitance of the second phospholipid monolayer to be calculated; for a DMPC/DMPS (7:3) monolayer it was determined to be $(2.1 \pm 0.7)\ \mu F\,cm^{-2}$.

The lipid bilayers thus prepared were used for binding experiments with MBP-Raf-C1, by means of the quartz crystal microbalance technique. A typical response of a 5 MHz quartz resonator before and after injection of the protein, with a final concentration of 0.3 μM, is depicted in Figure 3 A. The time of injection is set to zero. The immediate decrease in resonance

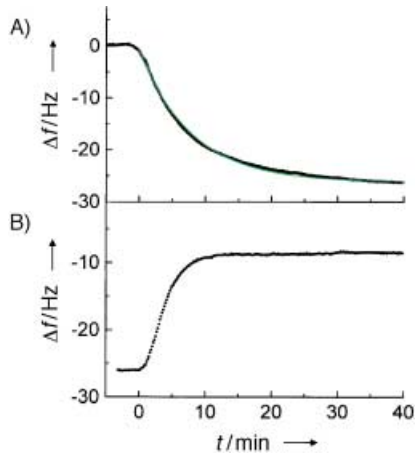

Figure 3. *A) Resonance frequency shift of a 5 MHz quartz surface functionalized with a lipid monolayer composed of DMPC/DMPS (7:3) physisorbed on an octanethiol monolayer. The time of injection is set to zero. A protein solution with a final concentration of 0.3 μM was added. The experiment was performed in PBS buffer (pH 7.4). The green line is the result of fitting the parameters of Equation (3) to the data. B) Response of the 5 MHz quartz plate after addition of a protease. After MBP-Raf-C1 had bound to the surface and the system had been thoroughly rinsed with buffer solution, Pronase E was added with a final concentration of 0.0125 mg mL^{-1}.*

frequency ($\Delta f = f(t) - f_0$) is indicative of protein adsorption to the lipid bilayer. After 40 minutes, an equilibrium frequency shift of 25 Hz has been reached. To ensure that protein had indeed been adsorbed onto the lipid bilayer, a protease, Pronase E, was added after protein binding was complete and the system was rinsed with buffer. As shown in Figure 3 B, the resonance frequency of the quartz increased by 16 Hz after injection of the protease; this indicates that bound protein was removed from the lipid interface. The frequency increase after protease digestion was 9 Hz less than the corresponding frequency decrease. This might be explained by protein material still remaining on the surface.

For a quantitative analysis of the kinetics of protein binding, we assumed that the rate-limiting step was the adsorption of the protein onto the surface, while diffusion-limiting steps were neglected, and that all individual protein binding sites were independent of each other (that is, no cooperativity took place). The binding kinetics can then be described by Equation (1), where $\Theta(t)$ is the surface coverage at any given time, K_d the dissociation constant of the monomolecular reaction, and c_0 the protein concentration of the bulk.

$$\Theta(t) = \frac{K_d^{-1} c_0}{1 + K_d^{-1} c_0}\left(1 - \exp\left(-\frac{t}{\tau}\right)\right) \quad (1)$$

τ is defined as the lifetime as in Equation (2), where k_{on} is the rate constant of association and k_{off} the rate constant of dissociation.

$$\tau(c_0) = \frac{1}{k_{on}\, c_0 + k_{off}} \quad (2)$$

Since the resonance frequency shift Δf is proportional to the amount of adsorbed material,[23] Equation (1) can be rewritten as Equation (3), where Δf_e is the equilibrium frequency shift for a given bulk protein concentration c_0.

$$\Delta f(t) = \Delta f_e\left(1 - \exp\left(-\frac{t}{\tau}\right)\right) \quad (3)$$

By fitting the parameters of Equation (3) to the data, the equilibrium frequency shift and the lifetime τ can be obtained. In Figure 3 A the result of the fitting routine is shown as a solid line with the corresponding parameters for $\Delta f_e = (25 \pm 1)$ Hz and $\tau = (480 \pm 20)\ s^{-1}$.

Determination of binding constants and rate constants for Raf-C1 binding to DMPC/DMPS

The experiment described above clearly shows that the interaction between MBP-Raf-C1 and solid-supported bilayers can be monitored in situ by means of the quartz crystal microbalance technique. To obtain the dissociation constants K_d and the rate constants of association and dissociation (k_{on} and k_{off}, respectively) protein concentration dependent measurements were performed on lipid bilayers composed of octanethiol and DMPC/DMPS (7:3). The concentration of MBP-Raf-C1 was varied between 0 – 16 μM and the equilibrium resonance frequency Δf_e and τ were extracted by fitting Equation (3) to the data. The results are shown in Figure 4 as plots of Δf_e versus c_0 (plot A) and τ versus c_0 (plot B). Fitting of a Langmuir adsorption isotherm [Eq. (4)] to the data shown in Figure 4 A results in a value for the

$$\Delta f_e(c_0) = \Delta f_{max}\frac{K_d^{-1} c_0}{1 + K_d^{-1} c_0} \quad (4)$$

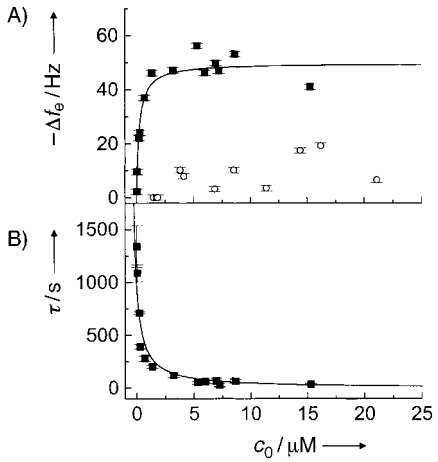

Figure 4. *A) Adsorption isotherm of MBP-Raf-C1 (■) and MBP (○). A lipid bilayer immobilized on a 5 MHz quartz plate composed of DMPC/DMPS (7:3) was used for each experiment. Δf_e and τ were obtained by fitting those parameters to the time course of the resonance frequency shift after addition of the corresponding amount of protein, by using Equation (3). By assuming a Langmuir adsorption isotherm [Eq. (4)], the dissociation constant K_d and the maximum frequency shift Δf_{max} were extracted. B) τ versus c_o plot. The rate constants of association and dissociation of MBP-Raf-C1 binding were determined by fitting Equation (2) to the data. The values are summarized in Table 1.*

dissociation constant of $K_d = (2.4 \pm 1.1) \times 10^{-7}$ M and a frequency shift Δf_{max} for maximum protein surface coverage of (50 ± 3) Hz.

Rate constants of association and dissociation were obtained by fitting Equation (2) to the data depicted in Figure 4B. The rate constants were determined to be $k_{on} = (2000 \pm 100)\ (\text{M s})^{-1}$ and $k_{off} = (10.5 \pm 0.3) \times 10^{-5}\ \text{s}^{-1}$. From the kinetics data, K_d can also be calculated by Equation (5) resulting in a value of $K_d = (5.4 \pm 0.3) \times 10^{-7}$ M.

$$K_d = \frac{k_{off}}{k_{on}} \qquad (5)$$

In order to ensure that the observed protein adsorption can be attributed to a specific binding of the Raf-C1 domain to phophatidylserine, we performed two different sets of control experiments. Firstly, we investigated the adsorption behavior of MBP-Raf-C1 onto neat DMPC. Up to concentrations of 3 μM, which would correspond to 92% coverage in the case of the adsorption of MBP-Raf-C1 to DMPC/DMPS (7:3), no significant frequency shift was observed. In the concentration range of 3–8 μM, a maximum frequency decrease of (8 ± 4) Hz was observed; this is well below the frequency shifts obtained for MPB-Raf-C1 bound to DMPC/DMPS (7:3). Secondly, we investigated the adsorption of maltose binding protein linked to the six histidine residues (MBP) onto DMPS-containing bilayers. Up to 2 μM of MBP, which corresponds to 89% coverage in the case of the adsorption of MBP-Raf-C1 to DMPC/DMPS (7:3), no frequency decrease was observed, while at higher concentrations a decrease in resonance frequency was registered (Figure 4A). The kinetics of MBP binding to DMPC/DPMS (7:3) were not reproducible. From our results we conclude that DMPS is the primary binding site for Raf-C1, while nonspecific adsorption of MBP onto DMPC/DMPS is only observed at higher protein concentrations.

Variation of the DMPS content

By varying the phosphatidylserine content we addressed the question of whether the DMPS content, and hence the effective negative surface charge density, affects the thermodynamic and kinetic parameters of Raf-C1 binding to the bilayer. We determined binding isotherms for bilayers containing 10 mol%, 30 mol%, and 100 mol% DMPS; the thermodynamic and kinetic data are summarized in Table 1. The most significant difference between the three bilayer systems under investigation is the increase in Δf_{max} with increasing DMPS content. The dissociation constants increased only slightly with increasing DMPS content, and no appreciable changes in the rate constants of association and dissociation were detected.

In order to investigate the maximum frequency decrease dependent on the DMPS content of the bilayer in more detail, we measured the maximum frequency shifts at protein concentrations above 5 μM. Independent of the DMPS content, this MBP-Raf-C1 concentration corresponds to a protein surface coverage of more than 90%, given the obtained dissociation constants of the three investigated bilayer compositions. To ensure that the quality of the lipid bilayer was not influenced by the lipid composition, the capacitance values were independently measured by impedance analysis. The results are summarized in Table 2. Except for bilayers composed of neat DMPS, the capacitance values were independent of the amount of negatively charged DMPS, with an average value of $C_{lipid} = (2.1 \pm 0.2)\ \mu\text{F cm}^{-2}$. The slightly larger capacitance value of a neat DMPS monolayer physisorbed onto an octanethiol monolayer might be due to the large surface charge density preventing tight packing of the lipids because of electrostatic repulsion and thus increasing the number of defects within the lipid monolayer. As defects would increase the amount of water molecules within the lipid monolayer, the mean dielectric constant and, therefore, the capacitance would be increased.

Table 1. *Thermodynamic and kinetic data of adsorption of MBP-Raf-C1 onto various lipid bilayers immobilized on gold surfaces of 5 MHz quartz plates.*

Acidic lipid content [mol%][a]	$-\Delta f_{max}$ [Hz]	K_d [M]	k_{on} [(M s)$^{-1}$]	k_{off} [s^{-1}]	K_d [M][b]
10 (PS)	19 ± 3	$(1.5 \pm 0.2) \times 10^{-7}$	$(1.4 \pm 0.1) \times 10^{3}$	$(5.5 \pm 0.9) \times 10^{-4}$	$(3.9 \pm 0.7) \times 10^{-7}$
30 (PS)	50 ± 3	$(2.4 \pm 0.1) \times 10^{-7}$	$(2.0 \pm 0.1) \times 10^{3}$	$(10.5 \pm 0.3) \times 10^{-4}$	$(5.4 \pm 0.3) \times 10^{-7}$
100 (PS)	96 ± 6	$(8.3 \pm 0.3) \times 10^{-7}$	$(1.8 \pm 0.2) \times 10^{3}$	$(10 \pm 1) \times 10^{-4}$	$(5.8 \pm 0.8) \times 10^{-7}$
30 (PG)	54 ± 6	$(3.2 \pm 0.2) \times 10^{-7}$	$(2.3 \pm 0.6) \times 10^{3}$	$(11 \pm 1) \times 10^{-4}$	$(4.8 \pm 1.3) \times 10^{-7}$

[a] PS: phosphatidylserine, PG: phosphatidylglycerol. [b] The dissociation constant was calculated from the obtained rate constants.

Table 2. *Capacitance values of octanethiol/phospholipid bilayers and phospholipid monolayers dependent on the DMPS content in the second phospholipid monolayer.*[a]

DMPS [mol%]	$C_{OT\text{-}lipid}$ [μF cm^{-2}]	C_{lipid} [μF cm^{-2}]
0	1.0 ± 0.2	2.2 ± 1.1
5	1.0 ± 0.1	1.8 ± 0.3
10	1.0 ± 0.1	1.8 ± 0.3
20	1.1 ± 0.2	2.3 ± 0.8
30	1.1 ± 0.2	2.1 ± 0.7
70	1.1 ± 0.1	2.2 ± 0.5
100	1.2 ± 0.2	3.0 ± 1.2

[a] The capacitances were obtained by fitting an equivalent circuit composed of a series connection of a capacitor and a resistance to the impedance data. The capacitance of the second phospholipid monolayer was calculated by assuming a series connection of the capacitance of the octanethiol and the phospholipid monolayer.

The maximum frequency shifts obtained for the different bilayer preparations are shown in Figure 5. A nonspecific adsorption with a mean frequency shift of (8 ± 4) Hz was observed, consistent with the binding of MBP-Raf-C1 to neat DMPC. With increasing DMPS content the resonance frequency

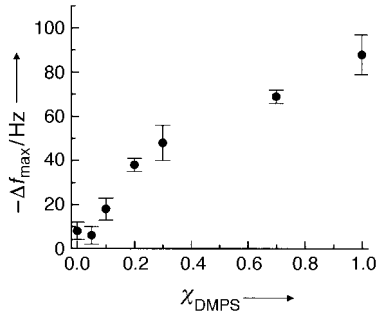

Figure 5. *Shifts in resonance frequencies dependent on the variation of the DMPS content in the second leaflet of the solid-supported bilayer. A MBP-Raf-C1 concentration of greater than 5 μM was added and the resonance frequency shift was extracted by fitting Equation (3) to the data.*

shift increased considerably. Up to a DMPS content of 30 mol% the increase in Δf was almost linear, leveling off at higher PS concentrations. The assumption of a linear correlation between the amount of adsorbed protein and the resonance frequency shift led to the conclusion that the surface was not fully covered with proteins even at high DMPS concentrations and that DMPS was essential for MBP-Raf-C1 binding. To support this hypothesis, we conducted scanning force microscopy imaging to view protein binding to a lipid membrane directly.

Scanning force microscopy (SFM)

From our previous studies we know that Langmuir – Blodgett (LB) layers composed of 1,2-dipalmitoyl-*sn*-glycero-3-phosphocholine (DPPC) and 1,2-dipalmitoyl-*sn*-glycero-3-phosphoserine (DPPS), deposited from a water or calcium ion containing subphase on a DPPC LB monolayer exhibit distinct round domains strongly enriched in DPPS.[24] These micrometer-sized domains are well suited for monitoring protein adsorption in situ.[25] Here, we attempted to use this well-defined system to investigate whether MBP-Raf-C1 binds solely to PS domains or whether it binds homogeneously to a lipid membrane and whether it binds as a monolayer. Figure 6 A shows a topographic

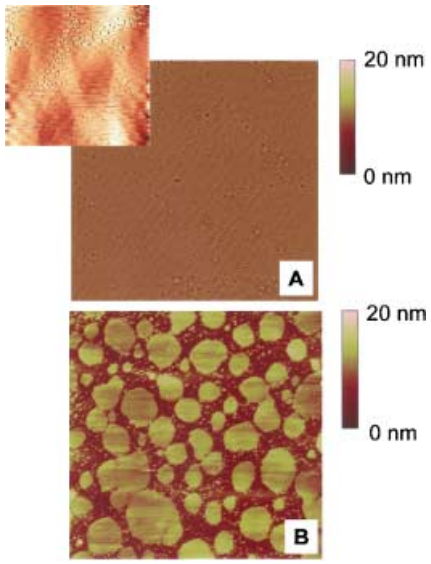

Figure 6. *A) Scanning force microscopy image of a DPPC – DPPC/DPPS Langmuir – Blodgett bilayer obtained in contact mode. The image size is 50 × 50 μm². The inset shows a lateral force microscopy image (backward scan) with a size of 34 × 34 μm². Dark areas are discernible and can be attributed to DPPS-enriched domains. B) Topographic image after addition of 5 μM MBP-Raf-C1. Bright, higher domains with varying sizes have become visible. Image size: 50 × 50 μm².*

image of a lipid bilayer composed of DPPC and DPPC/DPPS (4:1). The lipid bilayer appears rather flat, with some small defects discernible as dark spots. With the aid of lateral force microscopy, the more rigid DPPS-enriched domains can be visualized as darker areas in the backward scan direction (Figure 6 A, inset); this indicates stronger lateral forces at the darker domains. After incubation of the lipid layer with a 5 μM MBP-Raf-C1 solution for 30 minutes, domains with an increased height appear, and these can be attributed to adsorbed proteins (Figure 6 B). The adsorbed proteins were easily moved on the surface by applying higher load forces with the SFM tip. The load force of the tip had to be adjusted as low as possible to obtain good quality images. From the topographic images it can be concluded that the protein adsorbs as a monolayer and does not form multilayers; thus, the assumption of a Langmuir-like adsorption isotherm is justified. However, it is also evident that the protein preferentially binds to round, DPPS-enriched domains and is not homogeneously distributed on the surface. From lateral force microscopy imaging and secondary ion mass spectrometry, we know that approximately (30 ± 5) % of the overall area of the LB-layer is occupied by DPPS-enriched domains.[24, 25] Here, the protein coverage is (58 ± 5) %, considerably more than the area of the PS domains. This indicates that the protein does not only adsorb onto the negatively charged DPPS domains. It is conceivable that binding initially occurs at the negatively charged domains, while MBP-Raf-C1 over time becomes dis-

tributed over a larger area, due to lateral interaction of the proteins. There are also small brighter spots observable between the protein domains, which indicate MBP-Raf-C1 binding, probably to defects within the LB bilayer. A height analysis of the topographic images after adsorption of MBP-Raf-C1 reveals two distinct peaks (Figure 7). The peak difference corresponds to the protein height, which was determined to be (6.0 ± 0.3) nm, characteristic for a protein monolayer on the surface.

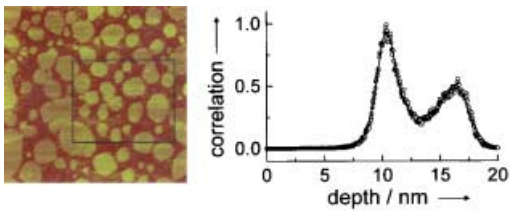

Figure 7. *Depth analysis (Gaussian filter) of the topographic image of the adsorbed protein domains on the lipid bilayers shown on the left. The area used for depth analysis is marked by a rectangle. Two well-separated height distributions, attributable to the protein layer and the lipid layer, respectively, were decomposed by fitting mixed Lorentzian/Gaussian functions to the data. The height difference between the two peaks was determined to be 6 nm.*

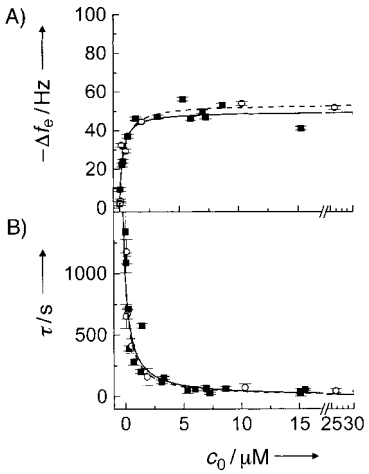

Figure 8. *A) Adsorption isotherm of MBP-Raf-C1 to a lipid monolayer composed of DMPC/DMPS (7:3) (■) and DMPC/DMPG (7:3) (○). The dissociation constant K_d and the maximum frequency shift Δf_{max} were extracted by fitting the parameters of Equation (4) to the data. B) τ versus c_0 plot. The rate constants of association and dissociation of Raf-C1 binding for DMPC/DMPS (7:3) and DMPC/DMPG (7:3) were determined by fitting Equation (2) to the data. The obtained parameters are summarized in Table 1. The solid (DMPC/DMPS) and broken lines (DMPC/DMPG) are the results of the fitting procedures.*

Interaction between MBP-Raf-C1 and phosphatidylglycerol

Since phosphatidylserine appears to be crucial for binding of MBP-Raf-C1 to lipid bilayers, we next addressed the question of whether the interaction between MBP-Raf-C1 and phosphatidylserine is specific and depends on the molecular structure of the lipid or whether binding is predominately electrostatically driven. For that purpose, we replaced DMPS with 1,2-dimyristoyl-*sn*-glycero-3-phosphoglycerol (DMPG), which has a net negative charge of -1, as DMPS does. A lipid mixture composed of DMPC/DMPG (7:3) was used for binding experiments. The obtained adsorption isotherm of MBP-Raf-C1, together with that of the adsorption of DMPC/DMPS (7:3), is depicted in Figure 8. Fitting of a Langmuir adsorption isotherm [Eq. (4)] to the data results in a value for the dissociation constant K_d of $(3.2 \pm 0.2) \times 10^{-7}$ M and a frequency shift Δf_{max} for maximum protein surface coverage of (54 ± 6) Hz, very similar to the values obtained for DMPC/DMPS. Rate constants of association and dissociation were obtained by fitting Equation (2) to the data and are also in the same range. The results are summarized in Table 1.

Discussion

The quartz crystal microbalance has been proven to serve as a versatile tool with which to quantify the interaction of proteins with lipid bilayers without adding a label to one of the components.[20, 26, 27] In this study, we used this technique to study the adsorption behavior of MBP-Raf-C1 with various phospholipid mixtures. It is postulated that the soluble protein Raf is recruited to the plasma membrane by interacting with lipid-anchored Ras, to result in the activation or channeling of its kinase activity.[5, 6] The driving force for this recruitment might be the interaction of the Raf – Ras binding domain with Ras and/or the interaction of Raf with the plasma membrane. Some publications favor the interaction of RafRBD and Ras.[3, 28, 29] However, Rizzo et al.[30, 31] recently demonstrated that the interaction of RafRBD and Ras is not crucial for membrane binding, but the interaction of a particular binding site located at the C terminus of Raf with phosphatidic acid is important. Others have demonstrated that the Raf-C1 domain is capable of interacting with phosphatidylserine membranes and have concluded that this might be the preferential binding site of the protein to lipid membranes.[12, 14, 18] To shed light on this, we determined thermodynamic and kinetic parameters characterizing the interaction of Raf-C1 with lipid bilayers. It turned out that the dissociation constant of MBP-Raf-C1 binding to lipid bilayers containing negatively charged DMPS was in the order of 100 – 800 nM. In comparison, the interaction of RafRBD with Ras was determined to be 130 nM under similar conditions and thus of the same order of magnitude.[32] It is conceivable that both domains, RafRBD and Raf-C1, anchor the protein to the lipid bilayer. Two separate interaction sites are advantageous in terms of the regulation of Raf kinase activity.

The Raf-C1 domain was already noted as a binding site for phosphatidylserine.[12, 14, 18] The results obtained in this study clearly indicate that the amount of PS within the lipid bilayer does not affect the binding affinity and kinetics of protein binding. However, the shift in resonance frequency accounting for the overall coverage is strongly influenced by the DMPS content in the lipid bilayer. The increase in resonance frequency shift with increasing DMPS content is indicative of the importance of PS for protein association. If there were a homogeneous distribution of DMPS within the DMPC matrix and one MBP-Raf-C1 bound to one PS molecule, an amount of 2 mol% of PS would be sufficient to cover the whole surface with protein. Since no

saturation took place up to 30 mol% and increases in frequency shift were still observable even at higher DMPS concentrations, we hypothesized that domain formation occurs on the surface.

We performed scanning force microscopy on a well-defined DPPC/DPPS mixture, to elucidate whether the protein binds only to PS-enriched domains or to both PS and PC. From the topographic images it was evident that the protein binds preferentially to the PS-containing domains, although the protein also covers areas containing PC. This supports the results of the quartz crystal microbalance measurements, in which little binding of Raf-C1 to pure DMPC was also found. The scanning force microscopy images also confirm that a monomolecular adsorption of the protein takes place, which validates the use of a Langmuir adsorption isotherm. Since aggregation of the protein occurs on the surface, it is conceivable that lateral interaction of individual proteins takes place. However, significant positive or negative cooperativity was not discernible from the adsorption isotherms.

The negative charge of phosphatidylserine appeared to be the crucial feature of this lipid acting as the binding site for MBP-Raf-C1. Replacement of DMPS with DMPG resulted in dissociation constants and kinetics of the same order of magnitude. The mainly electrostatic interaction of the protein with lipid bilayers was supported by scanning force microscopy; this demonstrates that higher loading forces move the proteins quite easily on the lipid surface, which is characteristic of weak electrostatic binding.

Conclusion

The quartz crystal microbalance (QCM) technique and scanning force microscopy (SFM) in combination with solid-supported lipid bilayers allow one to monitor the interaction of Raf-C1 with lipid membranes without labeling the protein component. Thermodynamic and kinetic data of the Raf-C1 lipid interaction were obtained by utilizing the QCM technique. As a spatially resolving technique, SFM enabled us to visualize the Raf-C1 binding sites directly at the membrane interface. From our results, it should now be feasible to localize the amino acids involved in the interaction of MBP-Raf-C1 with negatively charged lipids by mutagenesis experiments and to determine the changes in binding strength quantitatively.

Experimental Section

Materials: All reagents were used without further purification and were at least of p.a. grade. 1,2-dimyristoyl-*sn*-glycero-3-phosphocholine (DMPC), 1,2-dimyristoyl-*sn*-glycero-3-phosphoserine (DMPS), 1,2-dimyristoyl-*sn*-glycero-3-phosphoglycerol (DMPG), 1,2-dipalmitoyl-*sn*-glycero-3-phosphocholine (DPPC), and 1,2-dipalmitoyl-*sn*-glycero-3-phosphoserine (DPPS) were purchased from Avanti Polar Lipids (Alabaster, USA). Octanethiol was from Fluka, the gold used for the working electrodes, with a purity of 99.99%, was a generous gift from Degussa AG (Hanau, Germany), and the chromium was from Bal Tec (Balzers, Liechtenstein). Pronase E was obtained from Biochrom (Berlin, Germany).

Protein expression, isolation, and purification: The c-DNA of MBP-Raf-C1 (see Figure 1 B) corresponding to maltose binding protein and the amino acid residues 51 – 194, with an additional C-terminal His tag (six histidine residues), was cloned into a pMalc2 vector. The plasmid was transformed into *Escherichia coli* DH5α cells for protein expression. Expression was induced by 0.1 mM isopropyl-thio-β-D-galactopyranoside (IPTG) and the cells were grown at 18 °C. Twenty hours after induction, which was at the point of maximum expression, the cells were harvested. Lysis of the cells was achieved by ultrasonification, the suspension was centrifuged, and the supernatant was loaded onto an Ni^{2+}-charged HiTrap chelating HP column (Ni-NTA) column (Amersham Pharmacia, Freiburg, Germany). After washing with phosphate-buffered saline (20 mM phosphate buffer, 150 mM NaCl) containing 20 mM imidazole (pH 7.5), the protein was eluted with an imidazole gradient up to 500 mM; 5 mL fractions were collected. To prevent protein aggregation, dithiothreitol (20 mM) and $ZnCl_2$ (5 μM) were added to the samples and the pooled fractions were concentrated with centrifugal concentrators. The concentrated protein solution was further purified by size-exclusion chromatography (26/60 S.200 column, Amersham Pharmacia, Freiburg, Germany) in PBS buffer containing 20 mM imidazole and 5 μM $ZnCl_2$ (pH 7.5). After repeated concentration of the pooled protein fractions, the purified protein solution was dialyzed against PBS buffer (pH 7.5) at 4 °C, shock-frozen in liquid nitrogen, and stored at −70 °C. Protein concentration was determined by using the bicinchoninic acid (BCA) assay on microtiter plates according to the method of Smith et al.[33] The control protein MBP was expressed and purified in the same way.

Preparation of solid-supported bilayers on gold: Gold electrodes with an area of 0.33 cm^2 were deposited on each side of a quartz plate by means of an evaporation unit (E 306, Edwards, UK), by using a suitable mask design. After application of a layer of chromium (10 – 20 nm) to improve the adhesion of gold, the gold layer was subsequently deposited with a final thickness of about 200 nm. Prior to the incubation of the gold surfaces in the self-assembly solution, they were exposed to a high-energy argon plasma (plasma cleaner, Harrick, USA) for 5 – 10 min. After the quartz plate had been mounted in the measuring chamber, one of the two gold electrodes was exposed to an ethanolic solution of octanethiol (1 mM) for 30 min. Subsequently, the gold surface was first rinsed with ethanol and then with buffer solution. After an impedance spectrum has been taken to monitor the formation of the octanethiol monolayer, vesicles (0.5 – 1 mg mL^{-1}) of the corresponding composition were added. Vesicles exhibiting a mean diameter of 100 nm were prepared according to the extrusion method as described elsewhere.[34, 35] After incubation of the surface with the vesicle suspension for 30 – 90 min at 60 °C, a second phospholipid monolayer had been formed on top of the octanethiol monolayer, and an impedance spectrum was again taken to ensure proper formation of an insulating phospholipid monolayer.

Impedance analysis: A two-electrode setup was used for impedance analysis. The gold electrode with an area of 0.33 cm^2 evaporated onto a quartz plate served as the working electrode and a platinized platinum wire was used as counter-electrode. ac impedance analysis was performed with an impedance gain/phase analyzer from Solartron Instruments (Farnborough, UK). Impedance spectra ($|Z(\nu)|$, $\Phi(\nu)$) were recorded in a frequency range of 10^{-1} – 10^6 Hz with an ac amplitude of 30 mV.

Quartz crystal microbalance measurements: The QCM setup used in this study has been described in more detail elsewhere.[26, 27, 36] Briefly, we used highly polished, plano – plano, AT cut quartz resonators with a diameter of 14 mm and a fundamental resonance frequency of 5 MHz (KVG, Niederbischofsheim, Germany) with evaporated gold electrodes on both sides. The quartz plates were

mounted in a Teflon holder, exposing one side of the resonator to the aqueous solution. Both gold electrodes were connected to an oscillator circuit (SN 74LS 124N, Texas Instruments, Dallas, USA). An inlet and outlet allowed for a continuous buffer flow, by use of a peristaltic pump, and the addition of protein solutions. The flow rate was adjusted to 0.33 – 0.35 mL min^{-1}. The entire crystal holder was placed in a water-jacketed Faraday cage, thermostatted at 20 °C. The resonance frequency of the quartz resonator was monitored continuously with a frequency counter (HP 53181 A, Hewlett Packard, Palo Alto, USA) connected to a personal computer.

Preparation of Langmuir – Blodgett bilayers on mica: Langmuir – Blodgett (LB) films were prepared on a Wilhelmy balance with a 25 mL Teflon trough and a dipper device (Riegler & Kirstein, Berlin, Germany).[24] DPPC was spread on the water subphase and the lipid film was compressed at a rate of 1.8 $cm^2 min^{-1}$ to a surface pressure of 45 mN m^{-1}. The DPPC monolayer was transferred to a freshly cleaved mica sheet. A second monolayer composed of DPPC/DPPS (4:1) was then deposited onto the first hydrophobic DPPC monolayer at a surface pressure of 30 mN m^{-1}, and the mica sheet was transferred into an open fluid cell under water.

Scanning force microscopy: Scanning force microscopy (SFM) images were obtained in an open fluid cell with a Nanoscope III a Bioscope scanning force microscope (Digital Instruments, Santa Barbara, USA) operating in contact mode, equipped with a 100 × 100 μm^2 G-scanner. For topographical and lateral force images, microfabricated silicon nitride tips (NP-S, Digital Instruments, Santa Barbara, USA) with an approximate tip radius of 5 – 20 nm and a spring constant of 0.06 – 0.1 N m^{-1} were used as purchased. Minimal load force (200 – 400 pN) was employed during contact mode imaging, while the scan rate was set as high as possible (4 – 7 Hz for a 20 × 20 μm^2 image) to reduce the extent of bilayer deformation. For lateral force images, higher load forces in the range of 1 – 2 nN were applied.

The authors are very much indebted to B. Voß for her technical assistance. The research was funded by a DFG grant (Grant no.: BL 411/1 – 3) and the SFB (424).

[1] J. Avruch, X. Zhang, J. M. Kyriakis, *Trends Biochem. Sci.* **1994**, *19*, 279 – 283.
[2] G. Daum, I. Eisenmann-Trappe, H.-W. Fries, J. Troppmair, U. R. Rapp, *Trends Biochem. Sci.* **1994**, *19*, 474 – 479.
[3] D. K. Morrison, R. E. Cutler, *Curr. Opin. Cell Biol.* **1997**, *9*, 174 – 179.
[4] C. K. Weber, J. R. Slupsky, C. Herrmann, M. Schuler, U. R. Rapp, C. Block, *Oncogene* **2000**, *19*, 169 – 176.
[5] D. Stokoe, S. G. Macdonald, K. Cadwallader, M. Symons, J. F. Hancock, *Science* **1994**, *264*, 1463 – 1467.
[6] S. J. Leevers, H. F. Paterson, C. J. Marshall, *Nature* **1994**, *369*, 411 – 414.
[7] W. Kolch, *Biochem. J.* **2000**, *351*, 289 – 305.
[8] G. Heidecker, M. Huleihel, J. L. Cleveland, W. Kolch, T. W. Beck, P. Lloyd, T. Pawson, U. R. Rapp, *Mol. Cell. Biochem.* **1990**, *10*, 2503 – 2512.
[9] A. F. Quest, J. Bloomenthal, E. S. Bardes, R. M. Bell, *J. Biol. Chem.* **1992**, *267*, 10 193 – 10 197.
[10] A. F. Quest, E. S. Bardes, R. M. Bell, *J. Biol. Chem.* **1994**, *269*, 2961 – 2970.
[11] A. F. Quest, E. S. Bardes, W. Q. Xie, E. Willott, R. A. Borchardt, R. M. Bell, *Methods Enzymol.* **1995**, *252*, 153 – 167.
[12] S. Ghosh, W. Q. Xie, A. F. Quest, G. M. Mabrouk, J. C. Strum, R. M. Bell, *J. Biol. Chem.* **1994**, *269*, 10 000 – 10 007.
[13] J. H. Hurley, S. Misra, *Annu. Rev. Biophys. Biomol. Struct.* **2000**, *29*, 49 – 79.
[14] S. Ghosh, J. C. Strum, V. A. Sciorra, L. Daniel, R. M. Bell, *J. Biol. Chem.* **1996**, *271*, 8472 – 8480.
[15] H. R. Mott, J. W. Carpenter, S. Zhong, S. Ghosh, R. M. Bell, S. L. Campbell, *Proc. Natl. Acad. Sci. USA* **1996**, *93*, 8312 – 8317.
[16] A. Huwiler, J. Brunner, R. Hummel, M. Vervoordeldonk, S. Stabel, H. van den Bosch, J. Pfeilschifter, *Proc. Natl. Acad. Sci. USA* **1996**, *93*, 6959 – 6963.
[17] Y. A. Hannun, C. Luberto, *Trends Cell Biol.* **2000**, *10*, 73 – 80.
[18] T. Improta-Brears, S. Ghosh, R. M. Bell, *Mol. Cell. Biochem.* **1999**, *198*, 171 – 178.
[19] E. Sackmann, *Science* **1996**, *271*, 43 – 48.
[20] A. Janshoff, H.-J. Galla, C. Steinem, *Angew. Chem.* **2000**, *112*, 4164 – 4195; *Angew. Chem. Int. Ed.* **2000**, *39*, 4004 – 4032.
[21] T. Terada, Y. Ito, M. Shirouzu, M. Tateno, K. Hashimoto, T. Kigawa, T. Ebisuzaki, K. Takio, T. Shibata, S. Yokoyama, B. O. Smith, E. D. Laue, J. A. Cooper, *J. Mol. Biol.* **1999**, *286*, 219 – 232.
[22] A. Ulman, *Chem. Rev.* **1996**, *96*, 1533 – 1554.
[23] This is only valid for thinly adsorbed materials.
[24] M. Ross, C. Steinem, H.-J. Galla, A. Janshoff, *Langmuir* **2001**, *17*, 2437 – 2445.
[25] A. Janshoff, M. Ross, V. Gerke, C. Steinem, *ChemBioChem* **2001**, *2*, 587 – 590.
[26] A. Janshoff, C. Steinem, M. Sieber, A. el Baya, M. A. Schmidt, H.-J. Galla, *Eur. Biophys. J.* **1997**, *26*, 261 – 270.
[27] A. Janshoff, C. Steinem, M. Sieber, H.-J. Galla, *Eur. Biophys. J.* **1996**, *25*, 105 – 113.
[28] S. Roy, A. Lane, J. Yan, R. McPherson, J. F. Hancock, *J. Biol. Chem.* **1997**, *272*, 20 139 – 20 145.
[29] P. Dent, D. B. Reardon, D. K. Morrison, T. W. Sturgill, *Mol. Cell. Biol.* **1995**, *15*, 4125 – 4135.
[30] M. A. Rizzo, K. Shome, C. Vasudevan, D. B. Stolz, T.-C. Sung, M. A. Frohmann, S. C. Watkins, G. Romero, *J. Biol. Chem.* **1999**, *274*, 1131 – 1139.
[31] M. A. Rizzo, K. Shome, S. C. Watkins, G. Romero, *J. Biol. Chem.* **2000**, *275*, 23 911 – 23 918.
[32] C. Block, R. Janknecht, C. Herrmann, N. Nassar, A. Wittinghofer, *Nat. Struct. Biol.* **1996**, *3*, 244 – 251.
[33] P. K. Smith, R. I. Krohn, G. T. Hermanson, A. K. Mallia, F. H. Gartner, M. D. Provenzano, E. K. Fujimoto, N. M. Goeke, B. J. Olson, D. C. Klenk, *Anal. Biochem.* **1985**, *150*, 76 – 85.
[34] R. C. MacDonald, R. I. MacDonald, B. P. M. Menco, K. Takeshita, M. K. Subbarao, L. Hu, *Biochim. Biophys. Acta* **1991**, *1061*, 297 – 303.
[35] C. Steinem, A. Janshoff, W.-P. Ulrich, M. Sieber, H.-J. Galla, *Biochim. Biophys. Acta* **1996**, *1279*, 169 – 180.
[36] C. Steinem, A. Janshoff, J. Wegener, W.-P. Ulrich, W. Willenbrink, M. Sieber, H.-J. Galla, *Biosens. Bioelectronics* **1997**, *43*, 339 – 348.

Received: June 18, 2001 [F 256]